

An in-situ Degradation Behavior Study of MAO Coating on AZ91D Magnesium Alloy in Aqueous Solutions by SECM

Yan Xia¹, Zejie Zhu¹, Linrong Chang¹, Jianqing Zhang¹, Fahe Cao^{1,*}, Junxi Zhang²

¹ Department of Chemistry, Zhejiang University, Hangzhou 310027, China

² Shanghai Key Laboratory of Materials Protection and Advanced Materials in Electric Power, Shanghai University of Electric Power, Shanghai 200090, P. R. China

*E-mail: nelson_cao@zju.edu.cn

Received: 20 December 2016 / Accepted: 28 January 2017 / Published: 12 February 2017

The degradation behavior of AZ91D magnesium alloy with micro-arc oxidation (MAO) coating in NaCl solutions was studied by scanning electrochemical microscopy (SECM). The investigation was carried out at SECM with 10 micron tip using ferrocenemethanol (FcMeOH) as the redox mediator in feedback mode. The variation of localized reactivity of the MAO coating are reflected by tip currents in SECM mapping images, and the generation and evolution of active site/sites on MAO coating are correlated to the concentration of Cl⁻ in the solution and microstructure of the coating. With Cl⁻ concentration increasing, the rate of generation of active sites is accelerated and meanwhile the reactivity of the active sites is enhanced. For the relatively thick and porous coating, there are lots of independent active sites incubating, generating and evolving on coating with the extension of immersion time. While the coating is relatively thin and smooth, the coexistence of slender and lower current peaks and pieces of active regions appears. The reactivity of the artificial line scratch and surrounding areas varied with the increase of immersion time, indicating that the generation, accumulation and dissolution of corrosion product affect the corrosion behavior of AZ91 alloy.

Keywords: AZ91D; MAO coating; SECM; Feedback mode; Degradation behavior

1. INTRODUCTION

As a relatively new and efficient surface treatment technology, micro-arc oxidation (MAO) has been widely used in recent years to enhance the corrosion resistance of magnesium alloy [1-6]. After MAO treatment, a ceramic-like coating on the magnesium surface that is relatively thick and dense is produced. The protective properties of anodic coatings are determined by many factors, among which the composition and microstructure of the coating are extremely important. The main composition of

coating is MgO [7] and Mg(OH)₂ [8], both of which have an influence on the corrosion resistance of MAO coating due to their electric property and stability in aqueous solutions. The MAO coating is normally ceramic-like and porous, which contains various holes and cracks in it [9]. Simply speaking, the holes can be divided into through-holes and non-through-holes and the corrosion medium can transport through the former ones to arrive at the surface of the magnesium alloy, leading to the corrosion of magnesium alloy. The sites at which the corrosion medium can directly contact with the magnesium alloy and bring about the corrosion of the alloy are generally named weak sites, and the pitting corrosion at weak sites is the primary corrosion form of magnesium alloy covered by MAO coatings [10]. The investigation of the generation and evolution of active sites in weak sites is of great significance for us to deeply understand the degradation process of the MAO coatings.

Since pitting corrosion occurs at very small sites and suspends as soon as the electrolyte is taken away, it is hard to observe in situ the generation of active sites via conventional methods, like scanning electron microscope (SEM) and Atomic Force Microscope (AFM). Scanning electrochemical microscopy (SECM) is useful for investigating the gradually varied reactivity of the electrode surface of, because it can provide in-situ electrochemical information with high lateral spatial resolution [11]. The potential of SECM tip is set at a constant value far away of standard potential so that diffusion controlled electrochemical reaction of one electroactive specie takes place on it, and the tip current which is proportional to the concentration of the mediator and radius of tip is determined. When the biased tip approaches a substrate at close proximity, this current is deviated from the steady state limiting current $i_{T,\infty}$ collected in bulk solution, through either blockage of the diffusion of the electroactive species (negative feedback) or dominant regeneration of the reacted species from the substrate (positive feedback) [12]. It is possible to image the surface topography and/or chemical reactions on the surface by detecting the tip current as a function of spatial location when the tip is rastered in a plane close to the substrate. Early in 1990s, SECM was used to study the pitting corrosion behavior of Ti via monitoring the breakdown of the native or anodically grown oxide film and the evolution of electroactive sites on the substrate [13, 14, 15]. Then, Zhu et al. [16] quantitatively analyzed the reactivity difference between TiO₂ covered grain surfaces and Fe/Pd-containing boundaries at open circuit potential or bias potential. Serebrennikova et al. [17, 18] have reported the research of spatially localized electrochemical activity at Al/Al₂O₃ electrodes using SECM in order to establish the relationship between localized corrosion of Al (and Al alloys) with the defect structure of the native Al₂O₃ film. Souto et al. [19, 20] investigated the surface topography and degradation behavior of the organic coatings on metals, attacked by different anions. Generally in these researches, feedback mode was used and it is showed that we can distinguish active sites from non-active sites through the current response of the tip above the substrate. These SECM investigations provide a direct experimental demonstration of the relationship between electron transfer rates, oxide film conductivity and localized corrosion. Recently, the combination of SECM and other techniques has been used to study the corrosion of magnesium or Mg-based materials. Simões et al. [21] combined SECM and scanning electrode technique (SVET) to investigate the protection of an aluminum substrate by a Mg-rich coating, while the SVET has shown the evolution of the pit activity with time under sacrificial protection and the SECM allowed indirect sensing of the cathodic activity above the electrodes. Souto et al. [22] investigated the corrosion of an iron-magnesium galvanic couple with SECM in the

potentiometric and amperometric mode, using antimony and Mg^{2+} -ion selective electrodes as the tips. Then, they [23] used a new designed magnesium ion selective probe to image the concentration distributions of Mg^{2+} ions during the corrosion of the alloy AZ63. Substrate generation-tip collection mode of SECM was also used to study the effect of treatment time on the ionic liquid surface film on magnesium alloy AZ31 [24].

However, to our knowledge, there have been no in-situ measurements of the electrochemical behavior of magnesium alloy with MAO coating. In the current study, the micro-electrochemical behavior variations of magnesium alloy with MAO coating in aqueous solution with Cl^- was probed using SECM with feedback mode. SECM images were taken as a function of immersion time, which showed the reactivity variation of the substrate. The effect of Cl^- concentration, together with the composition and structure of coating itself on corrosion behavior of magnesium alloy with MAO coating were determined.

2. EXPERIMENTAL

The composition of AZ91D is the same as shown in our previous work [25]. The samples were mechanically cut into cylinders and embedded into PTFE, with a 0.2 cm^2 exposed surface area. The surface of the samples were gradually ground down to 1000 grit with SiC abrasive paper, then polished with a $0.5 \mu\text{m}$ diamond paste. After being degreased by acetone and washed with ultrapure water, the samples were anodized by a constant pulsed voltage power source for 3 min in the electrolyte containing $50.0 \text{ g}\cdot\text{L}^{-1}$ NaOH, $10.0 \text{ g}\cdot\text{L}^{-1}$ H_3BO_3 , $20.0 \text{ g}\cdot\text{L}^{-1}$ $\text{Na}_2\text{B}_4\text{O}_7\cdot 10\text{H}_2\text{O}$, $10.0 \text{ g}\cdot\text{L}^{-1}$ $\text{C}_6\text{H}_5\text{Na}_3\text{O}_7\cdot 2\text{H}_2\text{O}$, Na_2AlO_2 , Na_2SiO_3 and $2.0 \text{ g}\cdot\text{L}^{-1}$ organic additive. All those chemicals were reagent grade and were used as received. The detailed information of the device for anodization has been mentioned elsewhere in our group [25]. The frequency and duty cycle of the power source was set at 2000 Hz and 0.4 respectively, and two kinds of MAO coatings were obtained under the anodic oxidation voltage of 140 V and 100 V according to our previous work [26]. Ex-situ characterization of surface and scratch images before SECM tests was performed with TM3000 (Hitachi, Japan) scanning electron microscopy (SEM) with operation energy of 15 kV.

The SECM measurements were conducted by a CHI920C consisting of a three-axis positioning system driven by a motor and a bipotentiostat, so that the position of the tip electrode was controlled and the potentials of tip and specimen electrodes were independently controlled. A three electrodes configuration was used with a Pt ultramicroelectrode ($10 \mu\text{m}$ in diameter) tip as the working electrode, a Ag/AgCl, KCl (3 M) reference electrode and a platinum wire as a counter electrode. All potentials were referred to Ag/AgCl, KCl (3 M). In all SECM measurements, the substrate is AZ91D with MAO coating, and no bias potential is applied on the substrate.

The electrolyte solution for SECM tests contained 0.5 mM FcMeOH (A.R., Strem chemicals) as the redox mediator and 0.1 M or 0.62 M NaCl (S.P., Aladdin chemistry Co. Ltd) as the supporting and corrosive electrolyte. All aqueous solutions were prepared with ultrapure water ($>18 \text{ M}\Omega$, Milli-Q, Millipore).

Feedback mode was used in the probe approach curve and SECM mapping measurement, in which the tip potential was set at +0.45 V to monitor the oxidation of ferrocenylmethanol (FcMeOH) under diffusion control. The probe approach curves were fitted to the theoretical model for pure negative feedback behavior from COMSOL simulation according to our previous work [27] to get the exact tip-substrate distance. The scan rate of SECM imaging and line scanning was $40 \mu\text{m}\cdot\text{s}^{-1}$ and $30 \mu\text{m}\cdot\text{s}^{-1}$ respectively. All the experiments were performed at room temperature.

3. RESULTS

3.1 Surface micrographs of AZ91D with MAO coating

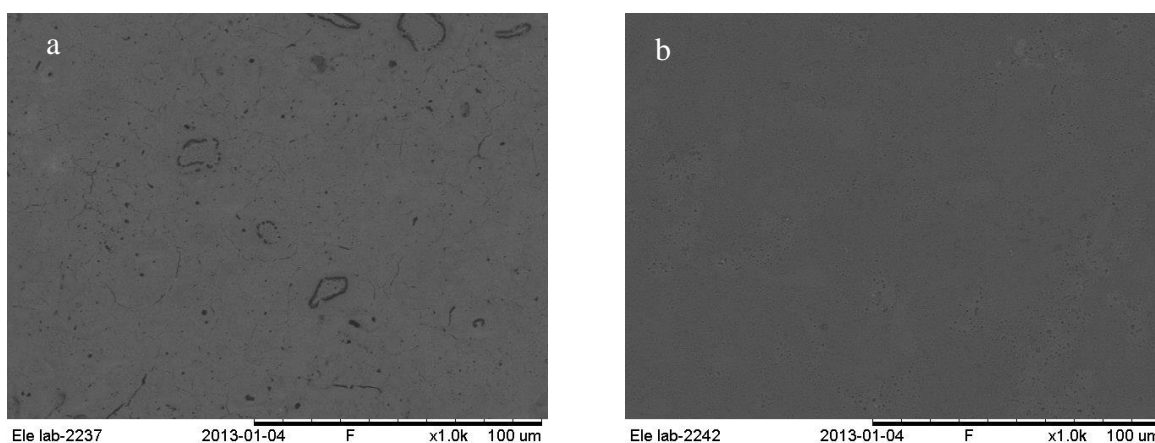


Figure 1. Typical SEM micrographs of the MAO coating anodized under different applied voltage: (a) 140 V and (b) 100 V.

As can be seen from surface morphologies in Fig. 1, there are much more pores and cracks on the MAO coating anodized under applied voltage of 140 V than that formed under 100 V, meanwhile the pore size of the former is relatively larger. Though, according to our previous work [26], the anodic coating obtained under voltage of 100 V is relatively smooth and uniform, which is much thinner than the coating obtained under anodic oxidation voltage of 140 V. Here, only two SEM surface images are shown in Fig. 1, more detail about the effect of applied voltage on the surface image of MAO coating on magnesium alloy can be found in many reported works, including our previous work. In the current research, two typical MAO coatings are used for SECM research, namely thin but smooth, and thick but coarse respectively, as shown in Fig. 1.

3.2 Probe approach curve on MAO coating

Since the main composition of the MAO coating consists of MgO and $\text{Mg}(\text{OH})_2$, which are nonconductive, it is expected that negative feedback response appears when the tip approaches to the MAO coating substrate. Fig. 2 shows that the probe approach curve of the tip approaching the MAO

coating substrate, which almost coincides with theoretical curve in pure negative feedback mode by COMSOL simulation, demonstrating no regeneration reaction of FcMeOH on the MAO coating and the insulating property of the MAO coating covered magnesium surface.

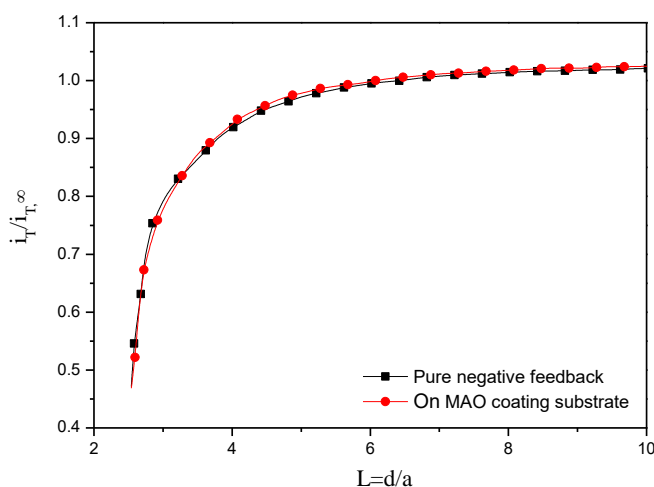


Figure 2. Probe approach curves to the MAO coating substrate recorded in 0.5 mM FcMeOH + 0.1 M NaCl aqueous solution with 10 μm Pt tip at a bias potential of 0.45 V vs. Ag/AgCl. The black square line is pure negative feedback curve based on COMSOL simulation.

3.3 The generation and evolution of active sites on MAO coatings

The SECM tip was set at a constant height of 4 μm above the MAO coating substrate based on the approach curve and rastered in the (X, Y) lateral plane to obtain SECM mapping images at different immersion time, with the scanning range 200 μm \times 200 μm . The tip was biased at 0.45 V while the substrate was left at open circuit potential.

Fig. 3 shows a series of SECM mapping images obtained over a magnesium alloy AZ91D substrate with MAO coating anodized at 140 V as a function of time in 0.5 mM FcMeOH + 0.62 M NaCl solution. Obviously, the dissolution of MAO coating covered substrate is inhomogeneous, and the tip currents are not uniform at different localized sites. As can be seen, the background current is around 6.1×10^{-10} A that is below than the steady state current ($i_{T,\infty}$) due to the negative feedback, indicating the insulating properties of the substrate, which is in line with the approach curve shown in Fig. 2. Some current peaks scatter on the matrix which is originated from the regeneration of FcMeOH on the substrate, reflects better conductive properties of the local sites, that is, the electrochemically active sites. With the increase of immersion time, the background current remains almost unchanged while the height and amount of current peaks varies a lot. Fig. 3a shows that after 0.5 h immersion in the NaCl solution, several local positions of MAO coating became active and a highly active site emerges, on which the current of the tip is greater than $i_{T,\infty}$. The conductive property of the active sites imply significant changes in the local chemistry environment, which is probably due to the breakdown of the MAO coating caused by attacking of chloride ions, and finally leading to parts of the AZ91D

alloy exposed to the solution. However, with the increasing immersion time to 1.5 h, the current peak disappears and a new current peak appears adjacent to it. Moreover, a number of peaks with slightly higher current than their surroundings background current are observed, which are probably generated by active sites in incubation period. With the extension of immersion time to 3.5 h, the density of the active sites increases significantly, and those formerly formed metastable active sites either evolved to highly active spots or gradually vanished with time. After soaked in NaCl solution for 5.5 h (Fig. 3d), the amount of active sites are considerably greater than before, indicating that the MAO was damaged seriously.

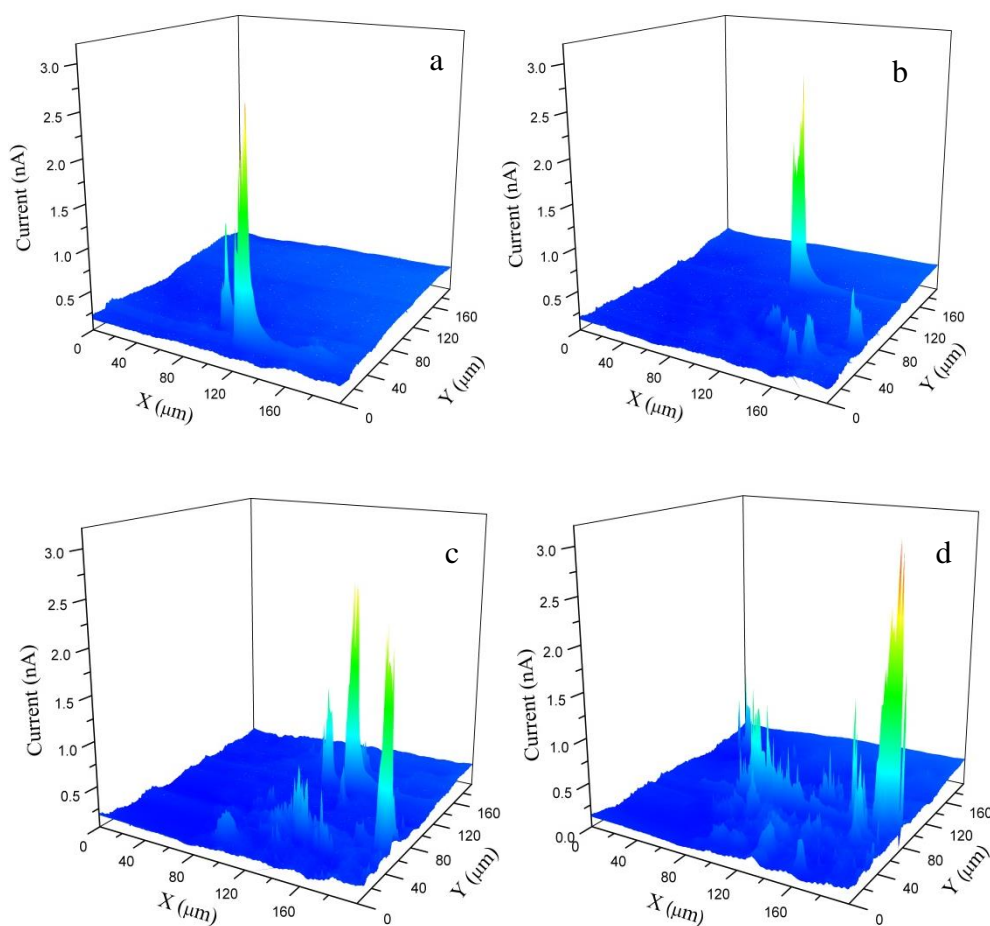


Figure 3. SECM images of magnesium alloy AZ91D with MAO coating anodized at 140V immersed in 0.5 mM FcMeOH + 0.62 M NaCl solution. The images were taken at different immersion time, (a) 0.5, (b) 1.5, (c) 3.5 and (d) 5.5 h.

Fig. 4 shows SECM images of magnesium alloy AZ91D with MAO coating anodized at 140 V immersed in 0.5 mM FcMeOH + 0.1 M NaCl solution. As can be seen, the generation and evolution

process of active sites on the MAO coating are similar to that in 0.62 M NaCl. Compare with those images obtained in 0.62 M NaCl, lower tip current peaks over the active spots are observed in 0.1 M NaCl, indicating that less AZ91D matrix exposed to the electrolyte due to the attack of fewer chloride ions. Besides, Fig. 4a shows that the tip current distributes uniformly without apparent variations in the scanning area, implying that the differences of the tip current were totally aroused by the topography changes of the MAO coating surface. As can be deduced from the distinction of Fig. 3 and Fig. 4, the concentration of Cl^- has a tremendous effect on the generation and evolution process of active sites on the MAO coating, in agreement with our previous research, that is, the dissolution and transformation of coatings can be accelerated with the concentration of Cl^- increased by FTIR measurement [25], which is not an in-situ technology.

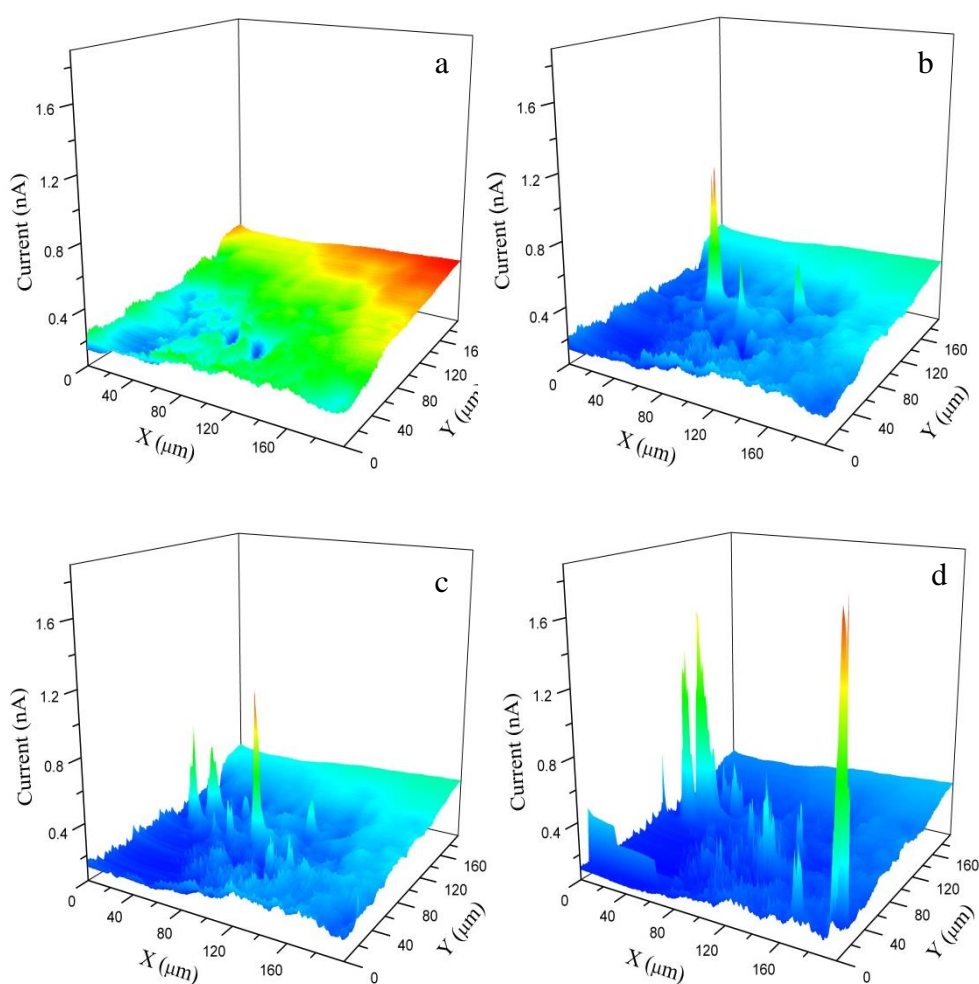


Figure 4. SECM images of magnesium alloy AZ91D with MAO coating anodized at 140V immersed in 0.5 mM FcMeOH + 0.1 M NaCl solution. The images were taken at (a) 0.5, (b) 1.5, (c) 3.5 and (d) 5.5 h after immersion in the solution.

To contrast the protective properties of the MAO coatings obtained under different applied voltages, the degradation process of magnesium alloy AZ91D with MAO coating anodized at 100 V immersed in 0.5 mM FcMeOH + 0.1 M NaCl solution was investigated. Similar to MAO coating anodized at 140 V, the uniformly distributed current after 0.5 h immersion (Fig. 5a) also reflects the information of the surface morphology of the MAO coating. After 1.5 h immersion, several current peaks are emerged which are more slender and weaker than that at 140 V. Meanwhile, the tip current was enhanced distinctly in a large area near the X axis, confirming the higher reactivity of this area than surroundings, which is not observed on the MAO coating anodized at 140 V. These observations probably correlated with the thin and compact properties of the MAO coating anodized at 100 V. With the immersion time increasing, the reactivity of the active area was slightly reduced and maintained at a steady state.

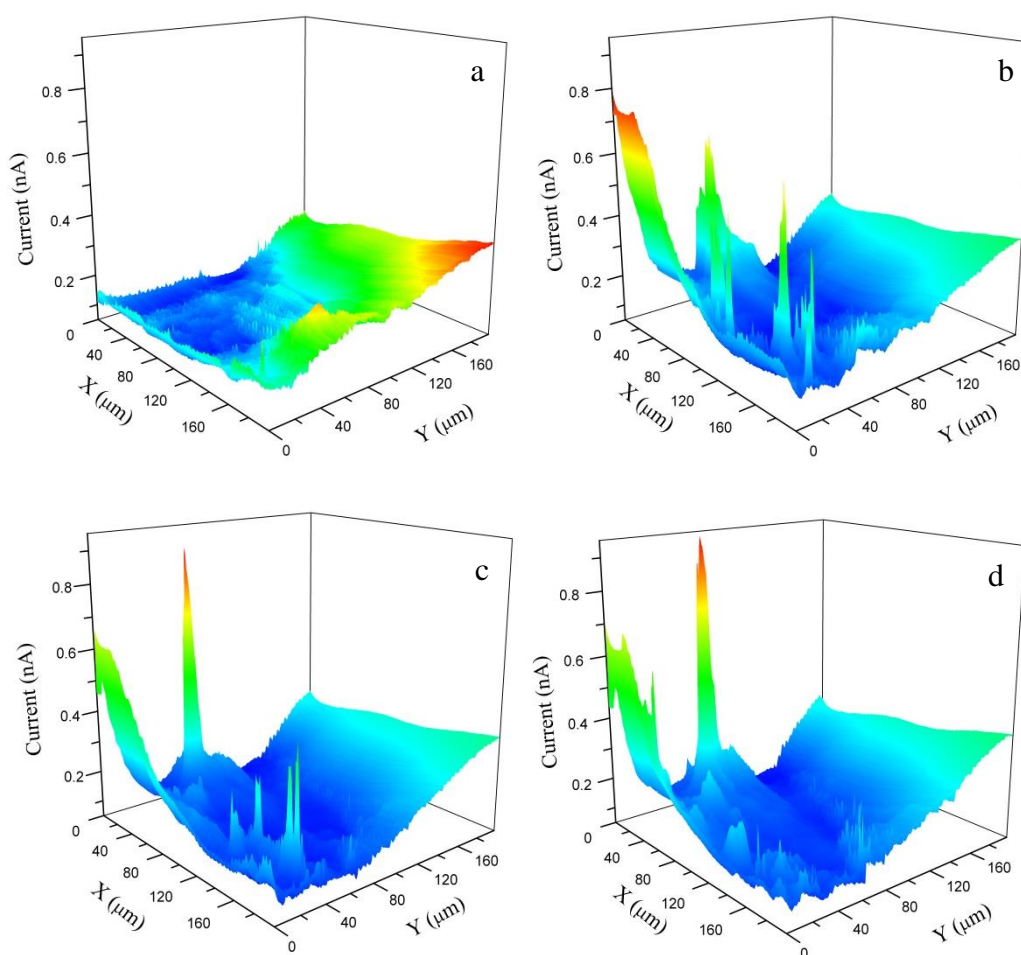


Figure 5. SECM images of magnesium alloy AZ91D with MAO coating anodized at 100V immersed in 0.5 mM FcMeOH + 0.1 M NaCl solution. The images were taken at (a) 0.5, (b) 1.5, (c) 3.5 and (d) 5.5 h after immersion in the solution.

3.4 The electrochemical activity of artificial scratches on MAO coating

Fig. 6 shows an artificial line scratch with the width of around 50 μm on the AZ91D alloy covered by MAO coating anodized at 140 V. The MAO coating at the scratch is totally disclosed so that the AZ91D alloy is exposed to the electrolyte directly. With the extension of the immersion time in aqueous solution, consecutive line scanning along X axis was conducted above the scratch, in which the tip-substrate distance and scanning length is 8 μm and 1200 μm respectively. Fig. 7 shows a series of scanning line curves over the scratches with different immersion time. As can be seen in Fig. 7a, the tip current above the scratch is enhanced markedly in contrast to the lower current over intact regions of the coating, indicating that the scratch still remain highly activity after 30 min immersion. At 40 min (Fig. 7b), the current of the tip above the scratch decreases, indicating the lowered activity of the scratch due to the corrosion production or film covered on the exposed AZ91D. Notably, there was a current peak around 250 μm , above where the tip current even exceeds that above the scratch, which should be caused by active sites. With the extension of the immersion time, the tip peak current around 250 μm gradually increases because of the enhanced reactivity of the sites. To the contrary, the tip current over the scratch decreased continually with the immersion time, and finally declined to the background value until 120 min, which was probably due to the covering of corrosion product to some extent. Moreover, as can be seen from above results, the existence of the scratch has no influence on the generation and evolution of the active sites adjacent to it, in other words, the active sites on the surface of MAO coating are independent to each other.

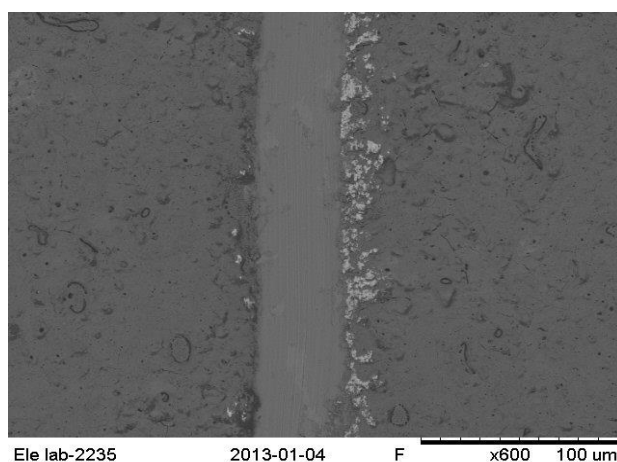


Figure 6. SEM surface images of the artificial scratch on AZ91D magnesium alloy with MAO coating.

Fig. 8 shows SECM images obtained over a region containing an artificial line scratch. The tip-substrate distance was set at 8 μm as same as the line scan experiment to avoid the probable crack of the tip to the anodic coating piling up at the edge of the scratch. There are some high current peaks in Fig.8 that reflect high reactivity of parts of the scratch range, coexistent with an amount of inversed current peaks appear over some other regions. The emerging of inversed current peaks was probably caused by the accumulation of the anodic coating which is insulated, so they reflect the morphology of these regions.

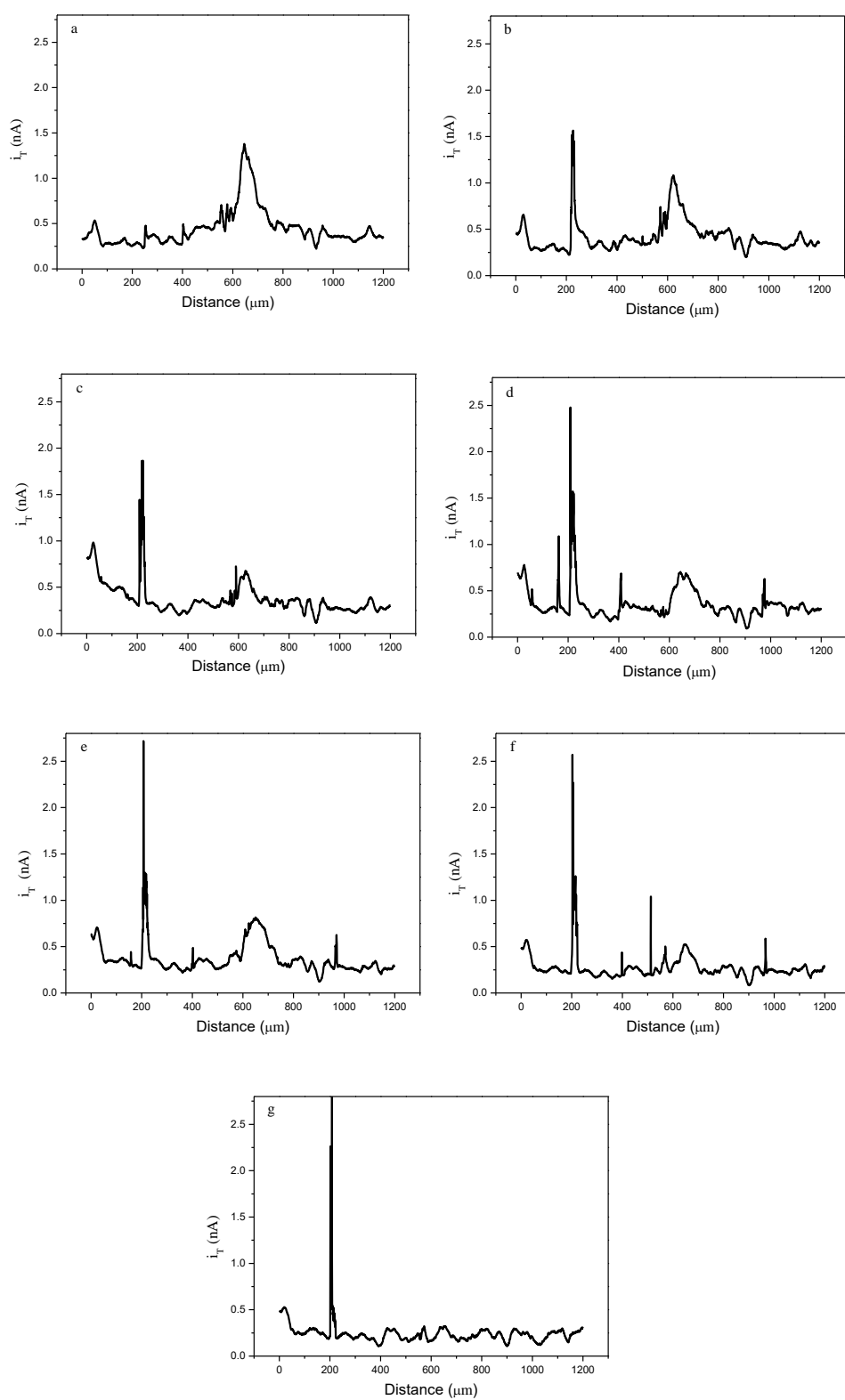


Figure 7 Scanning lines across an artificial scratch of magnesium alloy AZ91D with MAO coating immersed in 0.5 mM FcMeOH + 0.1 M NaCl solution for different time: (a) 30, (b) 40, (c) 50, (d) 60, (e) 70, (f) 80 and (g) 120 min.

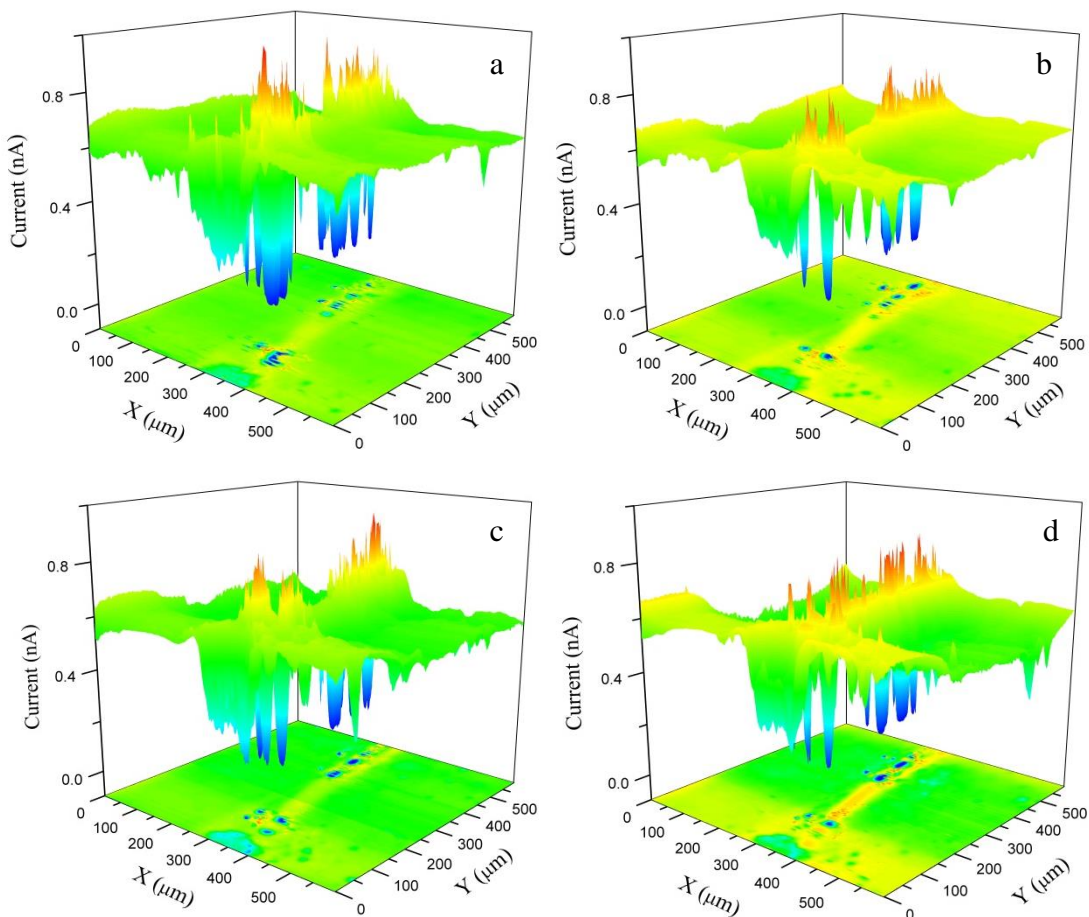


Figure 8. SECM images over the artificial scratch on AZ91D magnesium alloy with MAO coating immersed in 0.5 mM FcMeOH + 0.1 M NaCl solution. The images were taken at different immersion time, (a) 0.5, (b) 1.5, (c) 3.5 and (d) 5.5 h.

As the immersion time passed, the activity of the scratch was gradually reduced because of the accumulation of the corrosion product. The scratch and surrounding regions, regardless of the reactivity of them, are unstable and show great variation with the extension of immersion time. The results obtained above indicate that the generation, accumulation and dissolution of corrosion product have some effect on the corrosion behavior of AM91D alloy.

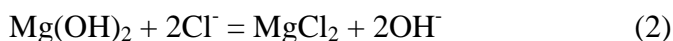
4. DISCUSSION

Our previous work has investigated the macroscopic corrosion of AM91D alloy covered by MAO coating and concluded that the mainly corrosion form is pitting corrosion [28]. The results indicates that the corrosion firstly occurs at locally weak sites like the defects of MAO coating, the formation and development of which are mainly form of degradation of AM91D alloy. Therefore, the macroscopic corrosion of AM91D alloy covered by MAO coating was correlated to the result of microscopic corrosion in this article. The reactivity variation of AM91D alloy covered by MAO

coating is partly caused by the generation and evolution of transformation regions on MAO coating [25]. At the initial stage of immersion in aqueous solution, there is lots of transformation regions formed, which seal numbers of micro-pores and cracks on the MAO coating. After 2 h immersion, transformation regions reduce and more micro-pores and cracks appear on the surface of anodic coating. These observations can account for the continually increased numbers and reactivity of active sites after 1.5 h immersion showed in the SECM results above. Compared to the SECM mapping of AM60 alloy without MAO coating [11], there are higher concentrated current peak can be found show in Figs. 3, 4 and 5, indicating the more severe localized corrosion appears due to the protection property of MAO coating on magnesium alloy. In addition to this, the explanation concerning the composition of MAO coating for the SECM observation is as follows. The main composition of MAO coating on AZ91D is MgO and Mg(OH)₂ which are unstable in neutral aqueous solutions, therefore, the MAO coating changes continually in NaCl aqueous solution. Since Mg(OH)₂ is thermodynamically more stable than that of MgO, MgO can spontaneously transform to Mg(OH)₂ via reaction equation (1), the Gibbs free energy of which is -26.989 kJ·mol⁻¹.



Mg(OH)₂ is not readily dissolved, and the molar volume of Mg(OH)₂ is larger than that of MgO, therefore, the protective property of the MAO coating is intensified at the very early stage of the immersion. Actually, the protective ability of Mg(OH)₂ is limited since it is unstable in neutral aqueous solutions especially containing Cl⁻, which can be absorbed on the surface of the coating and transform Mg(OH)₂ into soluble MgCl₂. The reaction of Mg(OH)₂ and Cl⁻ is shown as follows:



The dissolution of Mg(OH)₂ lead to the degradation of the MAO coating and the exposing of the bare alloy to the electrolyte, which account for the generation of the active sites and current peaks on the SECM images. Once exposed to the corrosion medium, AZ91D is dissolved via two approaches [29]: to form the soluble Mg²⁺ (equation 3) or an insoluble oxide/hydroxide film (equation 4).



Therefore, the active sites either are still active or covered by the accumulated Mg(OH)₂. In view of the porous structure of MAO coating, Mg(OH)₂ promotes the transformation of through holes to the non-through holes. Based on those discussions above, it can be concluded that the competition between the generation and the dissolution of Mg(OH)₂ is the primary cause of the mutual transformation of through holes and the non-through holes, in terms of SECM results, emerging and vanishment of active sites.

The different micro-electrochemical behavior of the two kinds of MAO coating formed with different applied potential can be attributed to their distinction in structures. The MAO coating obtained at 140 V has an average thickness of 15 μm while at 100 V the thickness is only 5 μm [26]. The micropores in the MAO coating obtained at 140 V are larger and greater in numbers than that at 100 V, which accounts for the greater numbers and higher reactivity of active spots. Comparatively speaking, the distinctive structure of 100 V coating bring about the coexistence of slender and lower current peaks and pieces of active regions.

5. CONCLUSIONS

The degradation behavior of AZ91D with MAO coating in NaCl solutions was studied by scanning electrochemical microscopy (SECM). The experimental results showed that the localized reactivity of the MAO coating varies from region to region, and the generation and evolution of active sites on MAO coating are correlated to the concentration of Cl⁻ in the solution and the structure of the coating. As the concentration of Cl⁻ increased, the rate of generation of active spots was accelerated and meanwhile the reactivity of the active spots was enhanced. For the relatively thick and porous coating, there are lots of independent active spots incubating, generating and evolving on it with the extension of immersion time. While the coating is relatively thin, there are pieces of active regions and a few of small active spots on the coating. The reactivity of the artificial scratch and surrounding areas varied with the increase of immersion time, indicating that the generation, accumulation and dissolution of corrosion product affect the corrosion behavior of AZ91 alloy.

ACKNOWLEDGEMENT

This work was supported by National Natural Science Foundation of China (Grant No. 51171172); Zhejiang Provincial Natural Science Foundation of China (Grant No. LR16E010001), Fundamental Research Funds for the Central Universities (Grant No. 2015QNA3011), Science and Technology Commission of Shanghai Municipality (No: 14DZ2261000) and the National Environmental Corrosion Platform.

References

1. T. Narayanan and M. Lee, *J. Alloys Compd.*, 687 (2016) 720.
2. H. Yu, Q. Dong, J. Dou, Y. Pan and C. Chen, *Appl. Surf. Sci.*, 388 (2016) 114.
3. H. Ardelean, I. Frateur, S. Zanna, A. Atrens and P. Marcus, *Corros. Sci.*, 51 (2009) 3030.
4. C. Wu, Z. Zhang, F. Cao, L. Zhang, J. Zhang and C. Cao, *Appl. Surf. Sci.*, 253 (2007) 3893.
5. F. Cao, L. Lin, Z. Zhang, J. Zhang and C. Cao, *T. Nonferr. Metal. Soc.*, 18 (2008) 240.
6. H. Tang and Y. Gao, *J. Alloys Compd.*, 688 (2016) 699.
7. H. Duan, C. Yan and F. Wang, *Electrochim. Acta*, 52 (2007) 3785.
8. V. Birss, S. Xia, R. Yue and R. Rateick, *J. Electrochem. Soc.*, 151 (2004) B1.
9. Z. Shi, G. Song and A. Atrens, *Corros. Sci.*, 47 (2005) 2760.
10. Y. Zhang, C. Yan, F. Wang and W. Li, *Corros. Sci.*, 47 (2005) 2816.
11. W. Liu, F. Cao, Y. Xia, L. Chang and J. Zhang, *Electrochim. Acta*, 132 (2014) 377.
12. A. Bard and M. Mirkin (2001). *Scanning Electrochemical Microscopy*. New York, Marcel Dekker.
13. S. Basame and H. White, *J. Phys. Chem.*, 99 (1995) 16430.
14. S. Basame and H. White, *J. Phys. Chem. B*, 102 (1998) 9812.
15. N. Casillas, S. Charlebois, W. Smyrl and H. White, *J. Electrochem. Soc.*, 140 (1993) L142.
16. R. Zhu, Z. Qin, J. Noel, D. Shoesmith and Z. Ding, *Anal. Chem.*, 80 (2008) 1437.
17. I. Serebrennikova and H. White, *Electrochem. Solid-State Lett.*, 4 (2001) B4.
18. I. Serebrennikova S. Lee and H. White, *Faraday Discuss.*, 121 (2002) 199.
19. R. Souto, Y. Gonzalez-Garcia, S. Gonzalez and G. Burstein, *Corros. Sci.*, 46 (2004) 2621.
20. J. Santana, J. Gonzalez-Guzman, L. Fernandez-Merida, S. Gonzalez and R. Souto, *Electrochim. Acta*, 55 (2010) 4488.
21. A. Simões, D. Battocchi, D. Tallman and G. Bierwagen, *Prog. Org. Coat.*, 63 (2008) 260.
22. J. Izquierdo, L. Nagy, I. Bitter, R. Souto and G. Nagy, *Electrochim. Acta*, 87 (2013) 283.

23. R. Souto, A. Kiss, J. Izquierdo, L. Nagy, I. Bitter and G. Nagy, *Electrochem. Commun.*, 26 (2013) 25.
24. Y. Zhang, X. Liu, S. Jamali, B. Hinton, S. Moulton, G. Wallace and M. Forsyth, *Surf. Coat. Technol.*, 296 (2016) 192.
25. L. Chang, F. Cao, J. Cai, W. Liu, J. Zhang and C. Cao, *Electrochem. Commun.*, 11 (2009) 2245.
26. L. Chang, F. Cao, J. Cai, W. Liu, Z. Zhang and J. Zhang, *T. Nonferr. Metal. Soc.*, 21 (2011) 307.
27. F. Cao, J. Kim and A. Bard, *J. Am. Chem. Soc.*, 136 (2014) 18163.
28. L. Chang, F. Cao, J. Cai, W. Liu, J. Zheng, J. Zhang and C. Cao, *Acta Phys.-Chim. Sin.*, 28 (2012) 127.
29. J. Świątowska, P. Volovitch and K. Ogle, *Corros. Sci.*, 52 (2010) 2372.

© 2017 The Authors. Published by ESG (www.electrochemsci.org). This article is an open access article distributed under the terms and conditions of the Creative Commons Attribution license (<http://creativecommons.org/licenses/by/4.0/>).